JACS
JOURNAL OF THE AMERICAN CHEMICAL SOCIETY

Subscriber access provided by ISTANBUL TEKNIK UNIV

Article

Nitrosonium Complexes of Resorc[4]arenes: Spectral, Kinetic, and Theoretical Studies

Bruno Botta, Ilaria D'Acquarica, Giuliano Delle Monache,
Laura Nevola, Danila Tullo, Franco Ugozzoli, and Marco Pierini

J. Am. Chem. Soc., **2007**, 129 (36), 11202-11212• DOI: 10.1021/ja072855i • Publication Date (Web): 17 August 2007

Downloaded from http://pubs.acs.org on February 14, 2009

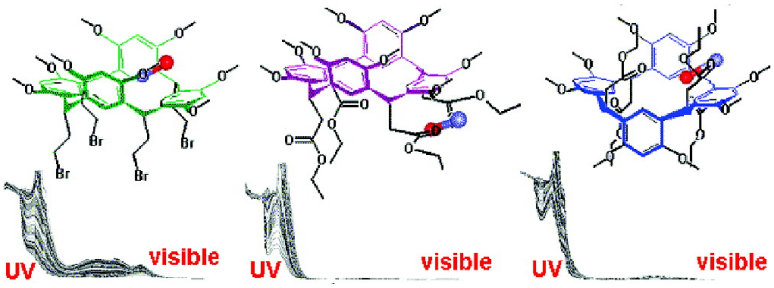

More About This Article

Additional resources and features associated with this article are available within the HTML version:

- Supporting Information
- Links to the 1 articles that cite this article, as of the time of this article download
- Access to high resolution figures
- Links to articles and content related to this article
- Copyright permission to reproduce figures and/or text from this article

View the Full Text HTML

ACS Publications
High quality. High impact.

Journal of the American Chemical Society is published by the American Chemical Society. 1155 Sixteenth Street N.W., Washington, DC 20036

J|A|C|S
ARTICLES
Published on Web 08/17/2007

Nitrosonium Complexes of Resorc[4]arenes: Spectral, Kinetic, and Theoretical Studies

Bruno Botta,*,† Ilaria D'Acquarica,† Giuliano Delle Monache,† Laura Nevola,† Danila Tullo,† Franco Ugozzoli,‡ and Marco Pierini*,†

Dipartimento di Studi di Chimica e Tecnologia delle Sostanze Biologicamente Attive, Università "La Sapienza", P.le A. Moro 5, 00185 Roma, Italy, and Dipartimento di Chimica Generale ed Inorganica, Chimica Analitica, Chimica Fisica, Università di Parma, Parco Area delle Scienze 17/a, 43100 Parma, Italy

Received May 2, 2007; E-mail: bruno.botta@uniroma1.it; marco.pierini@uniroma1.it

Abstract: Resorc[4]arene octamethyl ethers **1**−**3**, when treated with $NOBF_4$ salt in chloroform, form very stable 1:1 nitrosonium (NO^+) complexes, which are deeply colored. The complexation process is reversible, and the complexes dissociate and bleach upon addition of methanol or water, to give the starting macrocycles. Resorc[4]arenes **1** and **2** are in the same *cone* conformation, but with different side-chains, whereas **3** possesses a different conformation (*chair*), while bearing the same side-chain as **2**. Kinetic and spectral UV−visible analysis revealed that NO^+ interacts with resorc[4]arenes **1** and **2** both outside and inside their basket, leading to complexes with two absorption patterns growing at different rates, one featuring high-energy bands (HEB) within the near-UV zone, and the other one low-energy bands (LEB), attributed to charge-transfer interactions, within the visible range. The presence of ester carbonyl groups in **2** strongly drives the NO^+ cation outside the resorcarene. Resorc[4]arene **3** showed a spectral pattern pointing out a clear involvement of the ester moieties in the NO^+ entrapping, beside the formation of significant charge-transfer interactions. ^{1}H NMR spectroscopy and molecular modeling clearly supported these findings.

Introduction

Nitrogen dioxide (NO_2) belongs to the family of NO_X gases,[1,2] where NO_X is the general formula used to describe a mixture of NO_2, nitrogen monoxide (NO), and other nitrogen oxides. The unpaired electron on the nitrogen atom confers to NO_2 paramagnetic properties, an intense brown-orange color and the possibility of reacting with itself, to form a colorless dimer, dinitrogen tetroxide (N_2O_4).[3] N_2O_4 may disproportionate to ionic $NO^+NO_3^-$ upon reacting with aromatic compounds.[4] According to the capability of cations to strongly interact with the calixarenes π-surface,[5,6] very stable complexes between calix[4]arenes and nitrosonium (NO^+) cation have been described, both in solution and in the solid state, by Rudkevich,[7] Kochi,[8] and Rathore.[9] The NO^+ cation was found encapsulated within the calixarene cavity (X-ray analysis), and strong charge-transfer interactions with the π-surface of calixarene positioned the guest between the cofacial aromatic rings at a distance 2.4 Å, which is much shorter than the typical van der Waals contact (3.2 Å).[8] Resorc[4]arenes, similar to their relative calixarenes, are conformationally flexible molecules that can assume different stereostructures.[10] The *cone* conformation in solution is the result of an equilibrium between two *flattened cone* forms, in which two opposite aromatic rings are alternatively face to face. In most cases, at room temperature, the interconversion of the two structures (with C_{2v} symmetry) is fast on the NMR time scale and a simple spectrum corresponding to a C_{4v} symmetry is obtained.[11] Resorc[4]arenes in the *1,3-alternate* conformation are much more rigid and show two cofacial pairs of aromatic rings orthogonally oriented along the cavity axis.[7b] In the *cone* and *1,3-alternate* stereoisomer, all the substituents are axial (*rccc*). Conversely, in the *1,2-alternate* conformation, two neighbor rings point to one side and the two others to the

† Università "La Sapienza".
‡ Università di Parma.

(1) Lerdau, M. T.; Munger, J. W.; Jacob, D. J. *Science* **2000**, *289*, 2291−2293.
(2) Kirsch, M.; Korth, H.-G.; Sustmann, R.; de Groot, H. *Biol. Chem.* **2002**, *383*, 389−399.
(3) Addison, C. C. *Chem. Rev.* **1980**, *80*, 21−39.
(4) (a) Bosch, E.; Kochi, J. K. *J. Org. Chem.* **1994**, *59*, 3314−3325 and references cited therein. (b) Evans, J. C.; Rinn, H. W.; Kuhn, S. J.; Olah, G. *Inorg. Chem.* **1964**, *3*, 857−861.
(5) (a) Ikeda, A.; Shinkai, S. *J. Am. Chem. Soc.* **1994**, *116*, 3102−3110. (b) Ikeda, A.; Tsuzuki, H.; Shinkai, S. *Tetrahedron Lett.* **1994**, *35*, 8417−8420. (c) Ikeda, A.; Shinkai, S. *Chem. Commun.* **1994**, 2375−2376. (d) Ikeda, A.; Tsudera, T.; Shinkai, S. *J. Org. Chem.* **1997**, *62*, 3568−3574.
(6) (a) Asfari, Z., Böhmer, V., Harrowfield, J., Vicens, J., Eds. *Calixarenes 2001*; Kluwer Academic: Dordrecht, 2001. (b) Gutsche, C. D. *Calixarenes Revisited*; Royal Society of Chemistry: Cambridge, 1998. (c) Rudkevich, D. M. *Bull. Chem. Soc. Jpn.* **2002**, *75*, 393−413.
(7) (a) Zyryanov, G. V.; Kang, Y.; Stampp, S. P.; Rudkevich, D. M. *Chem. Commun.* **2002**, 2792−2793. (b) Zyryanov, G. V.; Kang, Y.; Rudkevich, D. M. *J. Am. Chem. Soc.* **2003**, *125*, 2997−3007. (c) Rudkevich, D. M. *Angew. Chem., Int. Ed.* **2004**, *43*, 558−571. (d) Rudkevich, D. M. *Kem. Ind.* **2005**, *54*, 57−63 and references cited therein.
(8) Rathore, R.; Lindeman, S. V.; Rao, K. S. S. P.; Sun, D.; Kochi, J. K. *Angew. Chem., Int. Ed.* **2000**, *39*, 2123−2127.
(9) Rathore, R.; Abdelwahed, S. H.; Guzei, I. A. *J. Am. Chem. Soc.* **2004**, *126*, 13582−13583.
(10) Botta, B.; Cassani, M.; D'Acquarica, I.; Misiti, D.; Subissati, D.; Delle Monache, G. *Curr. Org. Chem.* **2005**, *9*, 337−355.
(11) (a) Arduini, A.; Fabbi, M.; Mirone, L.; Pochini, A.; Secchi, A.; Ungaro, R. *J. Org. Chem.* **1995**, *60*, 1454−1458. (b) Conner, M.; Janout, V.; Regen, S. L. *J. Am. Chem. Soc.* **1991**, *113*, 9670−9671. (c) Scheerder, J.; Vreekamp, R. H.; Engbersen, J. F. J.; Verboom, W.; van Duynhoven, J. P. M.; Reinhoudt, D. N. *J. Org. Chem.* **1996**, *61*, 3476−3481.

10.1021/ja072855i CCC: $37.00 © 2007 American Chemical Society

Chart 1. Structure of the Resorc[4]arene Hosts

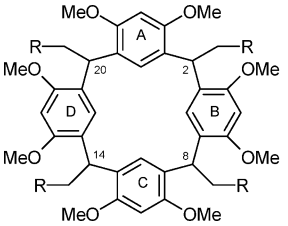

	R
1	CH_2Br (*cone*)
2	COOEt (*cone*)
3	COOEt (*chair*)

opposite (*rctc* substitution pattern). In the *chair* conformation, a pair of aromatic rings is almost in the same plane, whereas the others are orthogonally oriented up and down and facing the side-chains, which have a *rctt* substitution pattern.

Complexes of resorc[4]arenes with neutral molecules are generally weak, because the cavities themselves are too small; on the contrary, cations are known to more strongly interact with the resorcarene π-surface. Alkali metal cations and ammonium ions were shown to be complexed within the cone-shaped cavities.[12]

We have just found out that resorc[4]arenes **1**−**3** (Chart 1), when treated with NO_2, form stable NO^+-complexes, which are deeply colored and can dissociate and bleach upon addition of methanol or water, to give the parent resorc[4]arenes.[13] This paper deals with the kinetics of these host−guest complexes.

Results and Discussion

Choice of the Resorc[4]arene Hosts. At the beginning, we decided to evaluate the influence of different side-chain substitutions on the NO_X encapsulation using two resorc[4]arene hosts both in the *cone* conformation: the tetrabromide derivative **1** and the tetraester derivative **2** (Chart 1). Afterward, we extended the study to a third resorc[4]arene host (compound **3**) possessing a different conformation (*chair*), while bearing the same side-chain as host **2**. Resorc[4]arenes **2** and **3** were synthesized as previously described,[14a] starting from (*E*)-2,4-dimethoxycinnamic acid ethyl ester and using $BF_3{\cdot}Et_2O$ as the catalyst. Reduction of **2** yielded the corresponding tetraalcohol,[14a] which gave the tetrabromide derivative **1** by subsequent bromination.[14b] The *chair* conformation of compound **3** (initially interpreted as *1,3-alternate*)[14a] was definitively reassigned in the present paper by the obtainment of suitable crystals for X-ray analysis (see Supporting Information).

Interaction of Resorc[4]arenes 1−3 with NO_2. Bubbling NO_2 through chloroform solutions of resorc[4]arenes **1**−**3** rapidly resulted in deep purple (**1**) and violet (**2** and **3**) coloration. The UV−vis spectra showed the following charge-transfer bands: at λ_{max} = 545 and 628 nm for NO_2-exposed solution of **1**; at λ_{max} = 560 and 630 nm for solution of **2**, and at λ_{max} = 570 and 630 nm for solution of **3**. The intensity of the bands in the 545−570 nm range slightly decreased within 2 h and resembled the results obtained with NO^+ cation guest (from $NOBF_4$ salt) excess (*vide infra*).

Table 1. UV−Vis Data of Free Resorc[4]arenes **1**−**3** and Their NO^+ Complexes

species	[host]/[NO^+] ratio	λ (nm) of absorption bands	color
1	−	260; 284 (s)[a]	pale yellow
1−NO^+	≪1	260; 293 (s)[a]; 353; 628	deep purple
	≫1	260; 310; 341; 376 (s)[a]; 512; 573; 630	light purple
2	−	285	pale yellow
2−NO^+	≪1	248; 283; 340; 569[b]	deep violet
	≫1	260; 303; 341; 564; 629	light violet
3	−	260; 284 (s)[a]; 340	pale yellow
3−NO^+	≪1	263; 310; 340; 372 (s)[a]; 586; 623; (s)[a]	deep violet
	≫1	263; 312; 340; 365 (s)[a]; 569; 630	light violet

[a] (s) = shoulder. [b] Very weak band.

The dynamic interaction of resorc[4]arenes **1**−**3** with NO_2 showed very complicated ^1H NMR spectra of the corresponding solutions, difficult to monitor during the time, because of side-products derived from nitrosation/nitration reactions.[7b] The situation resembled the results obtained with NO^+ excess and will be fully discussed in another paper.

Interaction of Resorc[4]arenes 1−3 with Nitrosonium Cation. The formation of strongly colored adducts has been reported on complexation of calix[4]arene derivatives and NO^+ deriving from spontaneous NO_2 disproportion in chloroform.[15] To establish whether also in this case our hosts could entrap NO^+, qualitative experiments were designed in which the NO^+ cation (guest species) from $NOBF_4$ salt was added to chloroform solutions of resorc[4]arenes **1**, **2**, and **3** (host species). As expected, solutions become colored as in the case of bubbling NO_2, either when the host was in excess with respect to the guest and in the opposite case (see Table 1). The resorc[4]-arene−NO^+ complexes obtained resulted very stable and, in the absence of moisture, could be stored for several weeks, both in solution and in the solid state. Control experiments were also performed by mixing $NOBF_4$ with a chloroform solution of the starting monomer (*E*)-2,4-dimethoxycinnamic acid ethyl ester, used in the synthesis of resorc[4]arenes **1**−**3**. No color changes were observed by the time of the corresponding UV−vis spectra registration, thus proving the necessity of the supramolecular resorcarene structure for the NO^+ entrapment.

These preliminary experiments showing the tendency of resorc[4]arenes **1**−**3** to entrap NO^+ in stable colored adducts (***x***−NO^+ with ***x*** = **1**, **2**, and **3**) prompted us to study the matter in depth. For this purpose, a wide kinetic investigation on complexation between the resorc[4]arene hosts and NO^+ cation guest (from $NOBF_4$ salt) in chloroform was carried out, monitoring at 298 K the rate of absorption changes in the 300−700 nm UV−vis wavelength range. Two sets of experiments were performed: the first with an at least 10-fold excess host to guest, the second one with an at least 10-fold excess guest to host. The latter will be discussed in detail in another paper.

Host−Guest Complexation with a 10-Fold Excess Host to Guest. Resorc[4]arene 1. The kinetic pathway of the formation of **1**−NO^+ complex was monitored under pseudo-first-order conditions, recording in the 250−800 nm UV−vis wavelength range spectra of chloroform solutions containing a

(12) (a) Mäkinen, M.; Vainiotalo, P.; Rissanen, K. *J. Am. Soc. Mass Spectrom.* **2002**, *13*, 851−861. (b) Mäkinen, M.; Vainiotalo, P.; Nissinen, M.; Rissanen, K. *J. Am. Soc. Mass Spectrom.* **2003**, *14*, 143−151.

(13) Nunziata, A.; Lionetti, G.; Pierri, E.; Botta, B.; Cancelliere, G.; D'Acquarica, I.; Delle Monache, G.; Gasparrini, F.; Nevola, L.; Subissati, D.; Villani, C.; Cassani, M. Synthesis of resorcin[4]arenes and their use to adsorb nitrogen oxides from tobacco smoke. *PCT Int. Appl.* **2006**, 51 pp., WO 2006136950, Deposit 28.12.2006.

(14) (a) Botta, B.; Di Giovanni, M. C.; Delle Monache, G.; De Rosa, M. C.; Gács-Baitz, E.; Botta, M.; Corelli, F.; Tafi, A.; Santini, A.; Benedetti, E.; Pedone, C.; Misiti, D. *J. Org. Chem.* **1994**, *59*, 1532−1541. (b) Botta, B.; Delle Monache, G.; Ricciardi, P.; Zappia, G.; Seri, C.; Gacs-Baitz, E.; Csokasi, P.; Misiti, D. *Eur. J. Org. Chem.* **2000**, 841−847.

(15) Rosokha, S. V.; Kochi, J. K. *J. Am. Chem. Soc.* **2001**, *123*, 8985−8999.

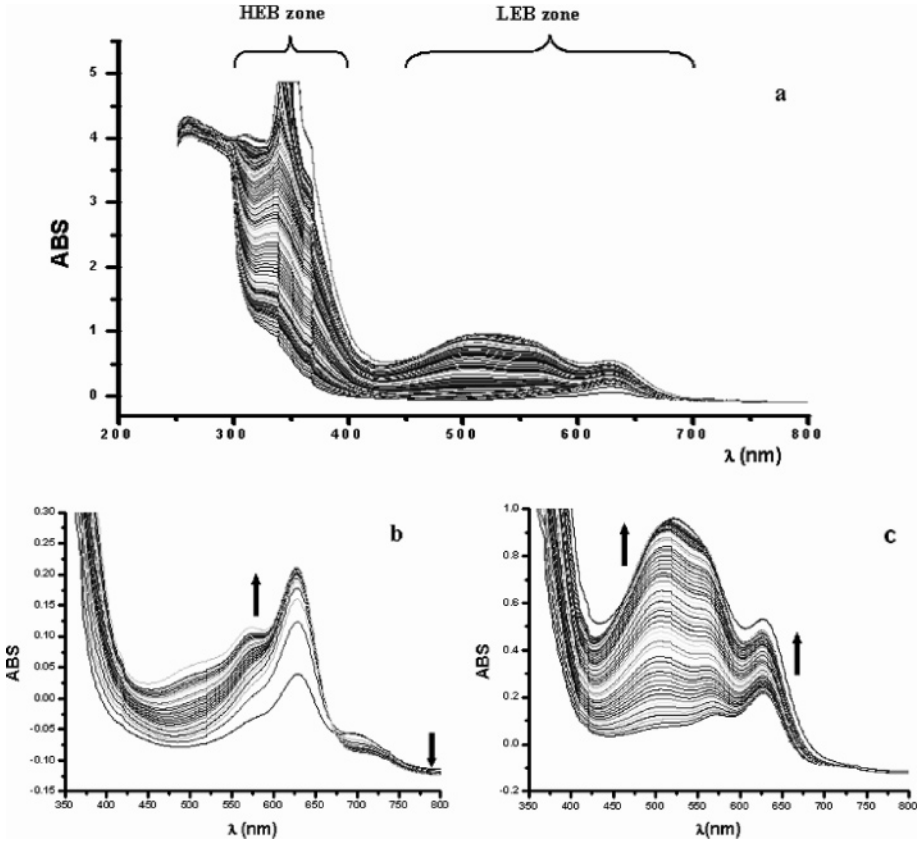

Figure 1. Superimposed UV−visible spectra obtained as a function of time from a chloroform solution containing **1**−NO^+ forming complexes at a host-to-guest molar ratio of 31. (a) All spectra recorded until the plateau achievement; ranges of high-energy bands (HEB) and low-energy bands (LEB) zones are schematically drawn over the data plot. (b) Ensemble of spectra recorded before the beginning of the absorbance (at 512 and 573 nm) increasing; an isosbestic point is visible at $\lambda = 669$ nm. (c) Ensemble of spectra recorded during the above absorbance increasing, until a definitive plateau was achieved.

host-to-guest molar ratio ranging from 10 to 31. Such conditions were chosen both to favor the formation of **1**−NO^+ complexes with a 1:1 stoichiometry and to simplify the mathematical treatment of the otherwise second order association process. Notably, at the equilibrium, two new wide absorption bands appeared (Figure 1a), the first in a region centered at λ_{max} 340 nm and large about 100 nm (high-energy bands, HEB zone), the second spanning the range 450−700 nm (low-energy bands, LEB zone). The two bands disappeared by addition of water and methanol, confirming the reversible trend of the complexation. According to Kochi *et al.*,[15] the absorption bands in the HEB zone are attributable to 1:1 complexes formed by NO^+ cation, located outside the macrocycle and leaned against an aromatic ring. Conversely, the bands appearing into the LEB zone should be due to complexes having NO^+ inserted into the cavity; in this case, the cation is expected to interact with two cofacial aromatic rings, thus establishing effective charge-transfer interactions.

The visible spectral changes recorded in the LEB region as a function of time were more clearly collected in two chronological ensembles (Figure 1b and 1c). In the first one (Figure 1b), the initial fast growth of the absorbance at 694 nm (5 min) is suddenly followed by a gradual decrease. Synchronic with this fall, a new absorbance band at 630 nm grows and achieves the plateau zone after 2 h (Figure 1b). The isosbestic point between the two curves visible in Figure 1b denotes interconversion phenomena occurring between two colored supramolecular species.

In the second ensemble of spectra (Figure 1c), slower but relevant increases of the absorbance at 512 and 573 nm were registered: both the curves reach the plateau zone after about 33 h, the first curve maintaining a slightly higher intensity than the second.

To monitor in details the initial fast growth of absorbance at 694 nm, its variation at different starting concentrations of **1** (from 3.5 to 0.8×10^{-2} M) was recorded every 5 seconds. Collected data were processed by nonlinear curve fitting analysis to determine the association rate constants (see Figure 1S in Supporting Information). Good correlation coefficients ($R^2 \geq 0.99$) were obtained in all cases considering the kinetic data as belonging to a first-order reversible process. The values of the obtained first-order rate constants are summarized in Table 2. A reasonable interpretation of these results can be proposed if the whole process is divided into three steps. In step I, corresponding to the absorbance growth at 694 nm, the rather unstable complex **1**−NO^+ is formed, according to a pseudo-first-order rate constant k'_{LEB} (I), since a very good linear correlation ($R^2 = 0.9997$) was achieved plotting the k'_{LEB} (I) values *versus* the corresponding initial host concentrations (from 3.5 to 0.8×10^{-2} M). From this plot, a second-order rate constant k''_{LEB} (I) $= 10.72 \pm 0.05$ min^{-1} M^{-1} for the formation of complex **1**−NO^+ was obtained as the slope of the interpolating straight line.

In step II, the presence of an isosbestic point is diagnostic for an actual interconversion between two isomeric forms of the complex. Accordingly, the same first-order rate constant

Table 2. First-Order Rate Constants (min^{-1}) of Resorc[4]arene−NO^+ Complexes

step	rate constants	host conc.	**1**–NO^+ complex	**2**–NO^+ complex	**3**–NO^+ complex
I	k'_{LEB} (I)	0.8×10^{-2} M	0.403 ± 0.030	0.0097 ± 0.0002	0.432 ± 0.011
		2.0×10^{-2} M	0.527 ± 0.017	–	–
		3.5×10^{-2} M	0.692 ± 0.018	–	–
II	k'_{LEB} (II)		0.120 ± 0.03	0.0026 ± 0.0001	0.0030 ± 0.0001
III	k'_{LEB} (III)		0.0037 ± 0.0004	–	–
	k'_{HEB}		0.0013 ± 0.0003	0.0108 ± 0.0002	0.0027 ± 0.0009

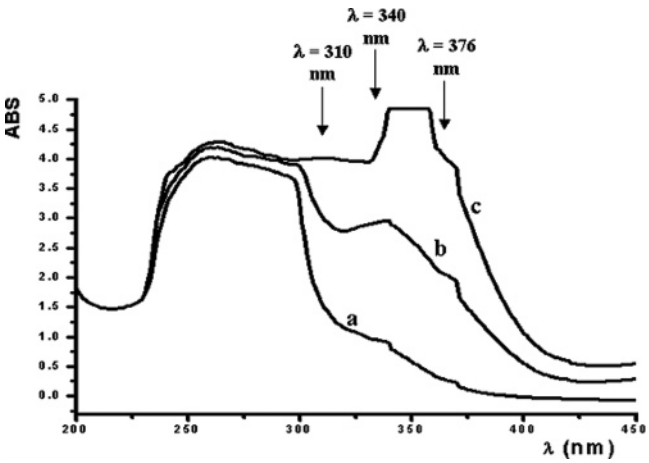

Figure 2. More relevant UV absorbance variations relative to the **1**−NO^+ adducts formation observable as a function of time in the HEB region. The a, b, and c spectra were registered at initial, intermediate, and final (achieved equilibrium) time, respectively.

[k'_{LEB} (II) = 0.120 ± 0.03 min^{-1}] was calculated both at 694 and 630 nm, independently on the starting host concentration.

Step III, a kinetically more complex phase of the process, was interpreted as due to a further rearrangement between the interacting host and guest, as it refers to a true first-order process. Rationally, in this step, different interconversion equilibria can exist, involving very similar and unstable **1**−NO^+ adducts, in which the guest molecule can assume different orientations, possibly into the host cavity, because the monitored absorbing bands are located in the LEB zone. In this case, the corresponding transition state should be represented by transient adducts with the NO^+ at the *upper rim*. This behavior could be attributed to a residual flexibility of the *cone* conformation. The kinetically complex variations of the spectral intensity observed in step III allowed a mathematical treatment only for the last portion of the process. The nonlinear curve fitting for such limited portion of the experimental data, performed at three different wavelengths (512, 573, and 630 nm), furnished, however, the corresponding average first-order rate constant [k'_{LEB} (III) = 0.0037 ± 0.0004 min^{-1}] with good correlation coefficients (R^2_{512} = 0.9952, R^2_{573} = 0.9916, R^2_{630} = 0.9964).

A kinetic study was also carried out for the variation of absorbance data in the HEB region, at 310 and 376 nm. The absorbance variation at these wavelengths, corresponding to a not sharp maximum and to a shoulder of the major band, respectively, enabled us to monitor the HEB region within the same conditions as the LEB zone (Figure 2). Again, good correlation coefficients (R^2_{310} = 0.9949, R^2_{376} = 0.9966) were obtained by interpolation of the data with a nonlinear curve fitting procedure according to a first-order kinetic treatment: the average value of the first-order rate constant of the process was k'_{HEB} = 0.0013 ± 0.0003 min^{-1}.

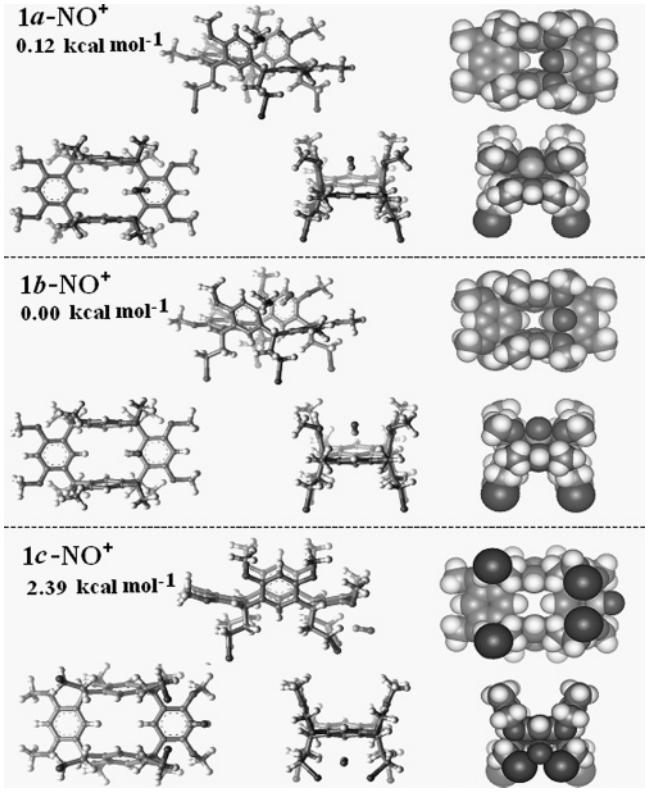

Figure 3. Ball-and-stick and CPK representations of the optimized geometries of **1**−NO^+ adducts obtained by semiempirical calculations. Energy values are relative to that of the most stable **1*b***−NO^+ adduct.

A theoretical rationale of the above results was obtained by semiempirical calculations. Optimized geometries of **1**−NO^+ complexes (Figure 3) were modeled starting from several different relative orientations of guest and host (in a *flattened cone* conformation) and taking into account the host/guest interactions, both inside and outside the resorcarene skeleton. In the calculations, the presence of the counterion (BF_4^-) was neglected to make an easier direct comparison among isomeric geometries, even though a fine estimation of the relative stabilities of the complexes was not possible. Within an energetic window of 3 kcal mol^{-1}, that is about 99% of Boltzmann probability, two very stable and highly populated geometries, **1*a***−NO^+ and **1*b***−NO^+, featuring the guest inside the cavity, were obtained. Conversely, in a third less stable geometry, **1*c***−NO^+, the guest was located outside, under the convex side of the resorcarene in the *lower rim* defined by the side-chain substituents.

In the **1*a***−NO^+ geometry (0.12 kcal mol^{-1}), the nitrogen atom is near to one of the flattened aromatic rings, while the oxygen atom is between the neighbor methoxyl groups of two opposite aromatic rings (Figure 3). In the **1*b***−NO^+ geometry (0.00 kcal mol^{-1}), the cation is instead tilted with its nitrogen

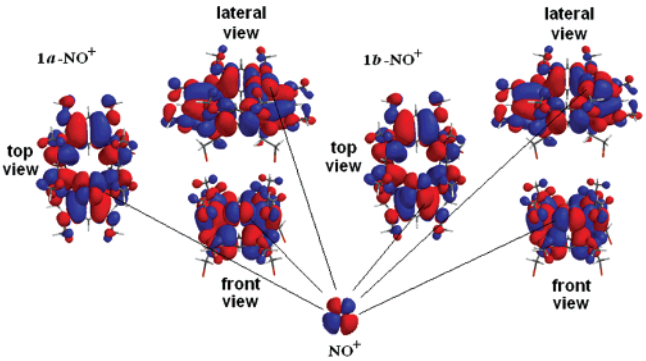

Figure 4. Pictures showing the favorable interactions between HOMO (host **1**) and LUMO (guest NO^+) orbitals in the **1*a***$-NO^+$ and **1*b***$-NO^+$ calculated adducts, seen from different points of view.

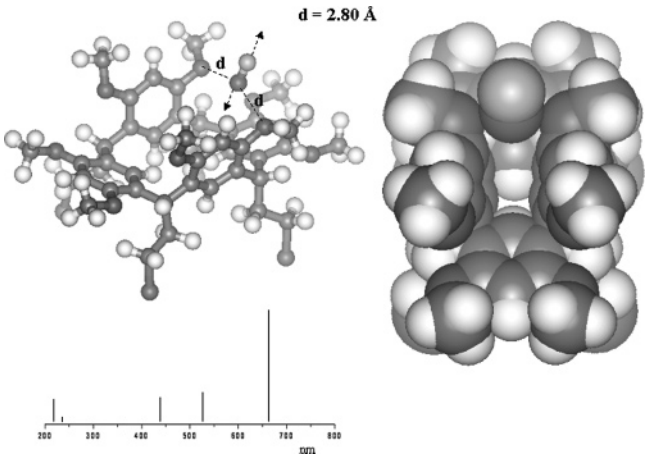

Figure 5. Picture showing (top) the model used to calculate the UV−vis spectra of hypothetical precursors of **1*a***$-NO^+$ and **1*b***$-NO^+$ adducts by the NO^+ approaching to the *upper rim* of host 1, and (bottom) the spectrum simulated when the distance among the oxygen atom of NO^+ and the oxygen atoms of the two methoxyl groups was equal to 2.80 Å.

atom pointing (down) toward the baricentre of the host, whereas the oxygen is still between the methoxyl groups of two rings face to face. In the last **1*c***$-NO^+$ geometry (2.39 kcal mol^{-1}), the nitrogen atom is pointing toward a flattened ring from outside and the oxygen is placed between the two adjacent bromoalkyl chains. These three adduct typologies seem to explain adequately both the UV spectral absorbances and the kinetic behavior (during the formation of the complexes themselves). The tight contacts between NO^+ and **1** in both **1*a***$-NO^+$ and **1*b***$-NO^+$ geometries suggest that charge-transfer interactions must be relevant to stabilize the complexes in agreement with the strong absorptions found in the LEB zone. Accordingly, the picture of the calculated HOMO and LUMO surface orbitals for the resorcarene and the nitrosonium cation revealed a favorable superimposition of the frontier orbitals in both **1*a***$-NO^+$ and **1*b***$-NO^+$ adducts (Figure 4).

In particular, stronger charge-transfer interactions were expected for the **1*b***$-NO^+$ complex, where the contact between NO^+ and the electronic clouds of the two cofacial aromatic rings was deeper and wider (see Figure 3). However, other relevant charge-transfer interactions were predictable, considering the overlapping between the Van der Waals surfaces of NO^+, of the pair of oxygens in the facing methoxyl groups and the neighbor flattened aromatic ring. Indeed, the superimposed UV−vis spectra of **1*a***$-NO^+$ and **1*b***$-NO^+$ complexes, evaluated by semiempirical calculation with ZINDO/s Hamiltonian, showed in the visible region quite similar absorbance peaks to the experimental data of free host **1** (Figure 2S in Supporting Information). In conclusion, significant adsorption bands over 600 nm are to be predicted for the **1*a***$-NO^+$ adduct, whereas more energetic and intense electronic transitions are expected in the simulated UV−vis spectrum of **1*b***$-NO^+$. Cumulatively, these considerations support the hypothesis that the LEB bands present in the experimental spectra of **1**$-NO^+$ adducts arise by NO^+ cation interacting with host **1** inside the cavity, thus maximizing charge-transfer contacts.

On consideration of the type of spectral changes observed during the formation of the **1**$-NO^+$ complexes by steps I−III, it may be supposed that adducts like **1*a***$-NO^+$ should be formed prior to complexes like **1*b***$-NO^+$. This claim also agrees with the major thermodynamic stability of **1*b***$-NO^+$, as compared with **1*a***$-NO^+$. To evaluate the hypothesis that **1*a***$-NO^+$ and **1*b***$-NO^+$ may be converted into each other in the experimental conditions, overcoming a not negligible energetic barrier, a molecular dynamic (MD) simulation was carried out. Indeed, the simulation revealed that the nitrosonium cation can tilt from the position of **1*a***$-NO^+$ and form the **1*b***$-NO^+$ adduct when the set temperature is ≥285 K, and vice versa when the set temperature is ≥300 K. The interconversion occurs through high energy states in which NO^+ is first aligned along the groove of the host *cone* conformation and then tipped over the *upper rim*. Other information was obtained by calculation of the UV−vis spectra of **1**$-NO^+$ adducts, in which the guest is placed outside the host, with the oxygen atom located between and interacting with two vis-a-vis methoxyl groups, within arrangements that might remind possible precursors of **1*a***$-NO^+$ and **1*b***$-NO^+$ adducts (Figure 5). As a result, a simulated absorption band at $\lambda > 600$ nm confirmed the charge-transfer interaction among three oxygen atoms (nitrosonium cation and two methoxyl groups), in coincidence with a distance minor than 3.18 Å. Such an instable adduct may be the actor of step I of the complexation process, before the inclusion of NO^+ in the resorcarene takes place.

Finally, we observed that the **1*c***$-NO^+$ adduct may well reproduce the typology of complexes, where the nitrosonium cation is coordinated outside the resorcarene cavity, because the tight contact between NO^+ and the external face of a flattened aromatic ring can be related with the minor absorption bands in the HEB zone. The coordination and entrapment of the cation require the cooperative movement of the two bromo alkyl chains and thus may explain the low formation rate of this complex (about three times slower than the one measured in step III).

$NOBF_4$ aliquots were added to a $CDCl_3$ solution of resorc-[4]arene **1**, and ^1H NMR spectra were run after each addition (see Figure 3S in Supporting Information). As a result, the signals of the free host (one signal for each type of proton, as required in a *cone* stereoisomer with a C_{4v} symmetry) were still present with slight changes but were flanked by smaller signals (about 15% of the main signals by integration), which were attributed to the **1**$-NO^+$ complex. Treatment with hexanes afforded a deeply colored, moisture-sensitive precipitate that exhibited a ^1H NMR spectrum where the satellite signals became prevalent and diagnostic. In Table 3, selected spectral data for the pure resorcarene **1** and the **1**$-NO^+$ complex are summarized.

Table 3. ^{1}H NMR Spectral Data (δ, ppm) of Free Resorc[4]arenes **1**−**3** and Their NO^+ Complexes

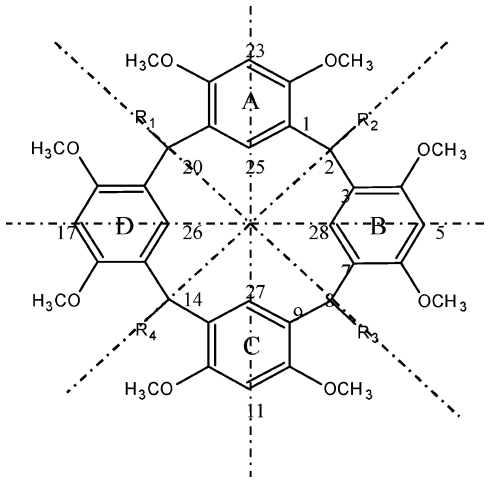

host	position/type	free resorc[4]arene	NO^+ complex[a]
1	25, 27; 26, 28	6.55 br s	6.45 s; 6.42 s
	5, 17; 11, 23	6.31 s	6.41 s; 6.38 s
	2, 14; 8, 20	4.60 t	4.62 t; 4.68 m
	OCH_3	3.63 s	3.87 br s, 3.75 br s
	CH_2Br	3.38 t	3.29 m
	$CH_2(CH_2Br)$	2.43 q	2.47 br q
2	25, 27; 26, 28	6.53 br s	6.87 br s, 6.84 s
	5, 17; 11, 23	6.31 s	6.39, 6.37, 6.35 s
	2, 14; 8, 20	4.96 t	4.96 br
	$O-CH_2(CH_3)$	3.83 q	4.24 q
	OCH_3	3.64 br s	3.75 s, 3.71 s
	$CH_2(COOEt)$	2.84 d	2.97 m
	$O-(CH_2)CH_3$	1.12 t	1.31 t, 1.17 t, 1.15 t (×2)
3	25, 27; 26, 28	6.82 br s, 6.20 br s	7.29 br s, 6.38 br s
	5, 17; 11, 23	6.46 s, 6.39 s	6.42 s, 6.41 s
	2, 14; 8, 20	5.01 dd	5.47 t, 5.12 t, 5.09 m (×2)
	$O-CH_2(CH_3)$	3.97 q	4.06 m, 3.97 m (×3)
	OCH_3	3.88 s, 3.65 s	3.85 s, 3.84 s, 3.78 s, 3.66 s
	$CH_2(COOEt)$	2.72 dd, 2.65 dd	2.98 dd, 2.86 dd, 2.87 d, 2.31 d
	$O-(CH_2)CH_3$	1.07 t	1.10 t (×3), 0.97 t

[a] Tentative assignments of selected signals.

In particular, the signal at δ 4.60 (t, $J = 7$ Hz) for the bridge methine protons (2, 8, 14, 20) of the guest-free **1** is split in the complex **1**−NO^+ into two signals, at δ 4.62 (t, $J = 7.5$ Hz) and 4.68 (m), respectively. The signal of H_e aromatic protons (5, 11, 17, 23) at δ 6.31 (s) of **1** is changed to two singlets at δ 6.41 and 6.38 in the complex. Analogously, the broad singlet of H_i aromatic protons (25, 26, 27, 28) at δ 6.55 in guest-free **1** becomes a couple of singlets at δ 6.45 and 6.42 in **1**−NO^+. Finally, the signal at δ 3.63 (s), accounting for the OCH_3 protons in **1**, was doubled at δ 3.87 and 3.75 in the complex **1**−NO^+. Cumulatively, the distribution pattern of the signals attributed to the **1**−NO^+ complex revealed that the entrapment of the cation reduced the symmetry of the resorcarene **1** from C_{4v} to C_{2v}. These findings agree with a location of the cation inside the cavity, suggesting two hypotheses: (i) NO^+ is oscillating, by an equilibrium exchange faster than the NMR time scale, between two equivalent positions over the two flattened aromatic rings; (ii) NO^+ is coordinated between the two co-facial aromatic rings, in a rigid and tight sandwich disposition. The optimized geometries **1*a***−NO^+ and **1*b***−NO^+ with C_S symmetry (Figure 3) obtained by the MM calculations and the complex evolution of the UV−visible spectral changes substantiate the first hypothesis.

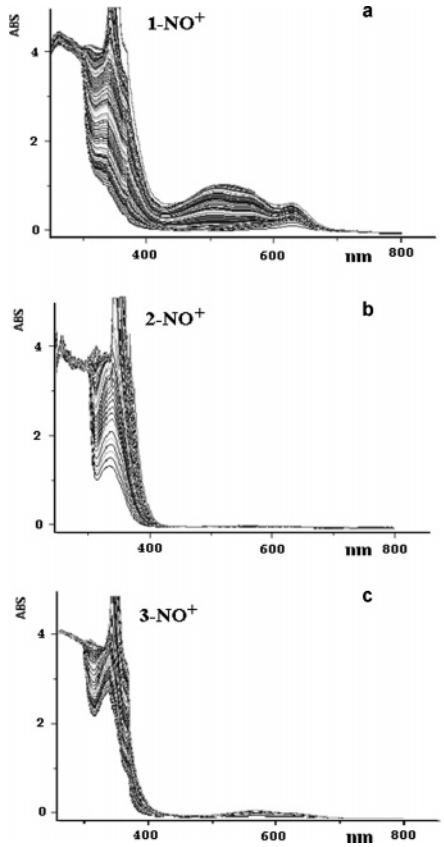

Figure 6. Comparison of experimental superimposed UV−vis spectra recorded as a function of time from chloroform solutions containing (a) **1**−NO^+, (b) **2**−NO^+, and (c) **3**−NO^+ forming complexes, at a host-to-guest molar ratio ≥10.

Resorc[4]arene 2. As in the case of **1**−NO^+ complexes, **2**−NO^+ chloroform solutions showed a mounting coloration by the time and bleaching by addition of water or methanol. Comparison of the UV−vis spectra of the mixtures at the equilibrium with those containing **1**−NO^+ complexes (Figure 6) revealed that the adducts adsorbing in the LEB zone (564 and 629 nm), that is, those attributed to complexes featuring the guest inside the macrocycle, are formed in very poor amounts.

Because resorc[4]arenes **1** and **2** differ from each other for the functionalization of the side-chain, this factor must be responsible of their different behaviors as hosts. Therefore, we supposed that the ester groups of **2** drive the nitrosonium cation outside the resorcarene, to give adducts with a geometry similar to **1*c***−NO^+, and are responsible for the absorption bands at 334 and 340 nm.

To support this claim, model geometries were optimized by semiempirical calculations starting again from host **2** in a *flattened cone* conformation (Figure 7). Indeed, two structures of **2**−NO^+ adducts with an external cation coordinated by the ester carbonyl groups, **2*c***−NO^+ (13.1 kcal mol^{-1}) and **2*d***−NO^+ (0.0 kcal mol^{-1}), were found to be much more stable than those with the guest inside the cavity, **2*a***−NO^+ (29.0 kcal mol^{-1}) and **2*b***−NO^+ (29.0 kcal mol^{-1}). This is particularly evident for the **2*d***−NO^+ model, where all four ester groups

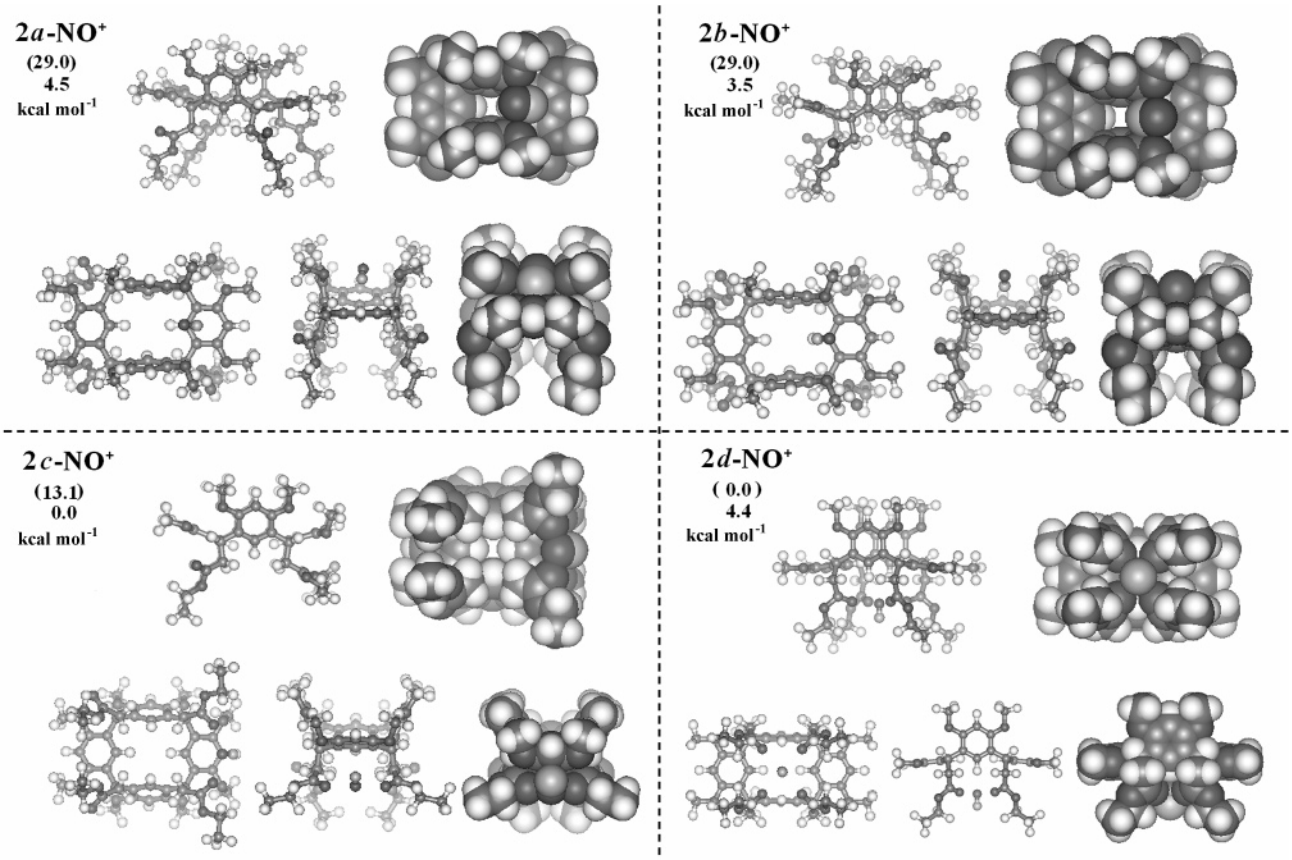

Figure 7. Ball-and-stick and CPK representations of the optimized geometries of **2**−NO^+ adducts obtained by semiempirical calculations. The numbers in parentheses are energy values not corrected for neither counterion presence nor entropic effects and are relative to that of the most stable adduct **2*d***−NO^+. The numbers below the parentheses are energy values corrected for both counterion presence and entropic effects and are relative to that of the found most stable adduct **2*c***−NO^+.

are engaged to coordinate NO^+. However, the presence of bands in the HEB region (300−400 nm) was not in agreement with the absence in **2*d***−NO^+ of interaction between NO^+ and the external π electronic cloud of an aromatic ring, whereas bands in the 300−400 nm region were expected from a **2*c***−NO^+ geometry. A persuasive explanation for this apparent incoherence between experimental and theoretical results is that the formation of adducts like **2*d***−NO^+ might be disadvantaged by both electrostatic and entropic reasons. In **2*d***−NO^+, in fact, the positive charge of nitrosonium cation can be delocalized to a higher extent than in the other adducts, where only two oxygen atoms are involved in the coordination. As a consequence, different stabilization effects for the interaction with the counterion BF_4^- should be involved for adduct **2*d***−NO^+ with respect to all the other ones, putting **2*d***−NO^+ at a disadvantage. Moreover, strong disadvantage for **2*d***−NO^+, but also in less extent for **2*c***−NO^+, should arise from the loss of internal rotational degrees of freedom for host complexation. Such an effect can be valuable[16] as about 32 u.e. on **2*d***−NO^+ (eight rotatable bonds constrained on its side-chains with respect to the adducts **2*a***−NO^+ and **2*b***−NO^+), and as about 16 u.e. on **2*c***−NO^+ (four rotatable bonds constrained on the side chains), that is, a $T\Delta\Delta S°$ contribution on $\Delta\Delta G°$ of complexation between **2*c***−NO^+ and **2*d***−NO^+ adducts of about 4.8 kcal mol^{-1} at 298 K, unfavorable to **2*d***−NO^+.

(16) Page, M. I.; Jencks, W. P. *Proc. Nat. Acad. Sci. U.S.A.* **1971**, *68*, 1678−1683.

A theoretical estimation of the claimed electrostatic interactions with the counterion was achieved by performing a further optimization of the **2**−NO^+ structures in the presence of BF_4^- placed in close proximity to the NO^+ cation in the complexes. The new energetic stability values of all the adducts, corrected for both counterion and entropic effects, are added in Figure 7. The **2*c***−NO^+ adduct widely resulted to be the most stable geometry, thus correctly accounting for the observed spectral profile in the HEB zone. In light of these findings, the meaning of the rate constants derived from the kinetic data for the **2**−NO^+ adducts formation could be better evaluated. The kinetic profiles recorded at $\lambda_{max} = 310$ nm (an absorbance minimum in the HEB zone), 564, and 629 (LEB zone) were interpolated with good correlation (R^2 values greater than 0.99) using reversible first-order kinetic equations (Figure 4S in Supporting Information). The measured rate constants k'_{LEB} (I) and k'_{LEB} (II) (average values of two determinations at 564 and 629 nm, respectively) and k'_{HEB} (310 nm) are collected in Table 2. All the rate constants turned out to be independent of host concentration (from 4.0 to 1.1×10^{-2} M), suggesting that the original formation step of **2**−NO^+ adducts occurs in shorter time than that we can monitor without the use of a stop-and-flow technique. Because this technique was unavailable to us, no determination of pseudo-first-order rate constant for the original **2**−NO^+ complex formation was possible.

Like in the formation of **1**−NO^+ adducts, the **2**−NO^+ complexes featuring the guest inside the host can be considered

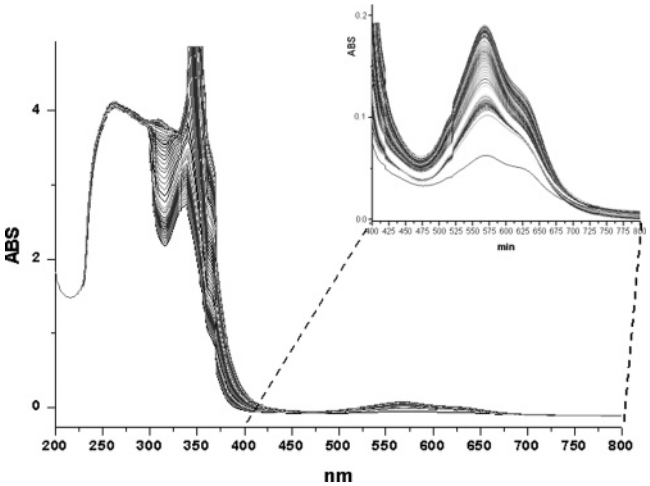

Figure 8. Superimposed UV−vis spectra obtained as a function of time from a chloroform solution containing **3**−NO^+ forming complexes at a host-to-guest molar ratio of 10. A magnification of the LEB zone is reported on the right side of the picture.

responsible for the different rate constants concerning the variations monitored in the LEB zone.

After addition of $NOBF_4$, a multitude of new signals, with different intensities (ranging from 5 to 15%), appeared in the ^{1}H NMR spectrum of resorc[4]arene **2** (see Table 3), but the precipitation with hexanes did not allow us to obtain a more informative spectrum, i.e., with increased signals for the **2**−NO^+ complex. A clear distribution pattern to be correlated with the results of the calculations was not obtained; however, the involvement of the substituents in the interaction with NO^+ can be deduced by the multiple signals for the side-chain ethyl ester moieties.

Resorc[4]arene 3. Chloroform solutions of **3**−NO^+, recorded by the time, generally showed more intense absorption bands in the HEB zone than in the LEB zone, quite similarly but less pronounced than **2** (Figure 8). In particular, two consecutive steps of increasing absorbance could be distinguished, step I (relative to $\lambda = 569$ nm in the LEB zone) being much faster than step II (relative to $\lambda = 312$ and 365 nm in the HEB zone and to $\lambda = 569$ and 630 nm in the LEB zone). The kinetic profiles corresponding to these steps were successfully simulated (with correlation coefficients R^2 greater than 0.996) using a first-order kinetic equation, as in the example reported in Figure 5S of Supporting Information. The rate constants k'_{LEB} (I), k'_{HEB} (average value of two determinations both at $\lambda = 312$ and 365 nm) and k'_{LEB} (II) (average value of two determinations both at $\lambda = 569$ and 630 nm) are collected in Table 2.

The independence of rate constants k'_{LEB} (I), k'_{HEB}, and k'_{LEB} (II) on the host concentration (from 2.4 to 0.8×10^{-2} M) suggests that the kinetic processes registered both in the HEB and in the LEB zone should correspond to first order rearrangements of the adduct geometries generated during a not registered bimolecular initial step. Furthermore, because the $k'_{HEB} = 0.0027 \pm 0.0009$ min^{-1} and k'_{LEB} (II) $= 0.0030 \pm 0.0001$ min^{-1} values result to be identical within the experimental error, it seems logical to consider them as the evolution of the same process. Thus, the whole kinetic pathway concerning the formation of **3**−NO^+ complexes can be rationalized distinguishing two phases, the first corresponding to the initial fast formation and rearrangement of a relatively unstable **3**−NO^+ adduct, and the second involving slow changes of the adduct geometry, directed to maximize the host−guest interactions. Because in the *chair* conformation of host **3** there is not a cavity available to entrap the guest between two aromatic rings (like in the sandwich dispositions already met with ***1a***−NO^+ and ***1b***−NO^+ complexes), it is not easy to envisage from which kind of **3**−NO^+ geometry the visible absorptions registered in LEB zone can arise. However, we may suppose the formation of highly feasible adducts having the NO^+ cation disposed among an aromatic ring and the carbonyl groups of two ester moieties, in a fashion similar to that one shown by the calculated ***2c***−NO^+ geometry. Notably, the structure of such kind of adducts would be perfectly consistent with the new absorptions registered in the HEB zone.

To obtain more information about the favored points of contacts between **3** and NO^+, semiempirical calculations to design **3**−NO^+ adducts were performed by the same procedure used for **1**−NO^+ complexes. The host input structure was the X-ray generated *chair* conformation of resorc[4]arene **3** (see Supporting Information). Five most stable geometries (***3a***−***e***−NO^+) were obtained within an energetic window of 4 kcal mol^{-1} (Figure 9). Three of the found adducts (***3a***−NO^+, ***3b***−NO^+, and ***3d***−NO^+) placed NO^+ at the same time over the plain of the two horizontal aromatic rings and among one of the vertical aromatic rings and two ester carbonyl groups of the side-chains (^{in}**3**−NO^+ disposition type). By contrast, within the other two adducts (***3c***−NO^+ and ***3e***−NO^+), NO^+ is disposed outside the host structure (^{out}**3**−NO^+ disposition type), interacting again with one of the two vertical aromatic rings and two carbonyl groups of ester moieties that act on cation in a bidentate way. The two most stable adducts of ^{in}**3**−NO^+ type differ for the orientation of nitrosonium cation, which points its oxygen toward the inner (***3a***−NO^+) or the outer (***3b***−NO^+) of the host molecule. These geometries represent together a very large (>99%) Boltzmann population and may account for the spectral absorptions of **3**−NO^+ solutions in the LEB zone. Indeed, in both cases, NO^+ is not symmetrically disposed with respect to the host molecule, but it appears slightly tilted with its external atom (that is, nitrogen in ***3a***−NO^+ and oxygen in ***3b***−NO^+) pointing toward the near oxygen atoms of a methoxyl group and of two carbonyl groups. At the same time, the internal atom of the nitrosonium cation (oxygen in ***3a***−NO^+ and nitrogen in ***3b***−NO^+) is at a tight contact with a reduced portion of two neighbor perpendicular aromatic rings. The favorable superimposition, with a complete accordance of the phase signs, between HOMO orbital of **3** and LUMO orbital of NO^+ in ***3a***−NO^+ adduct (Figure 10), can establish the charge-transfer interactions responsible for the absorptions in the LEB spectral range. The not optimal performance of this cofacial interaction may also account for the moderated absorbance intensities of these bands as compared with those shown in the HEB zone. In the simulated spectra of ***3a***−NO^+ (Figure 6S in Supporting Information) are present absorption bands both in the HEB (313 nm) and in the LEB zone (560 nm), in agreement with the experimental observations.

In spite of a quite remarkable difference between the host conformations (*cone* for **1** and *chair* for **3**), without considering the side-chains substitution, the kinetic pathways concerning the formation of **1**−NO^+ and **3**−NO^+ revealed a notable similarity. Both the processes are characterized by a fast initial

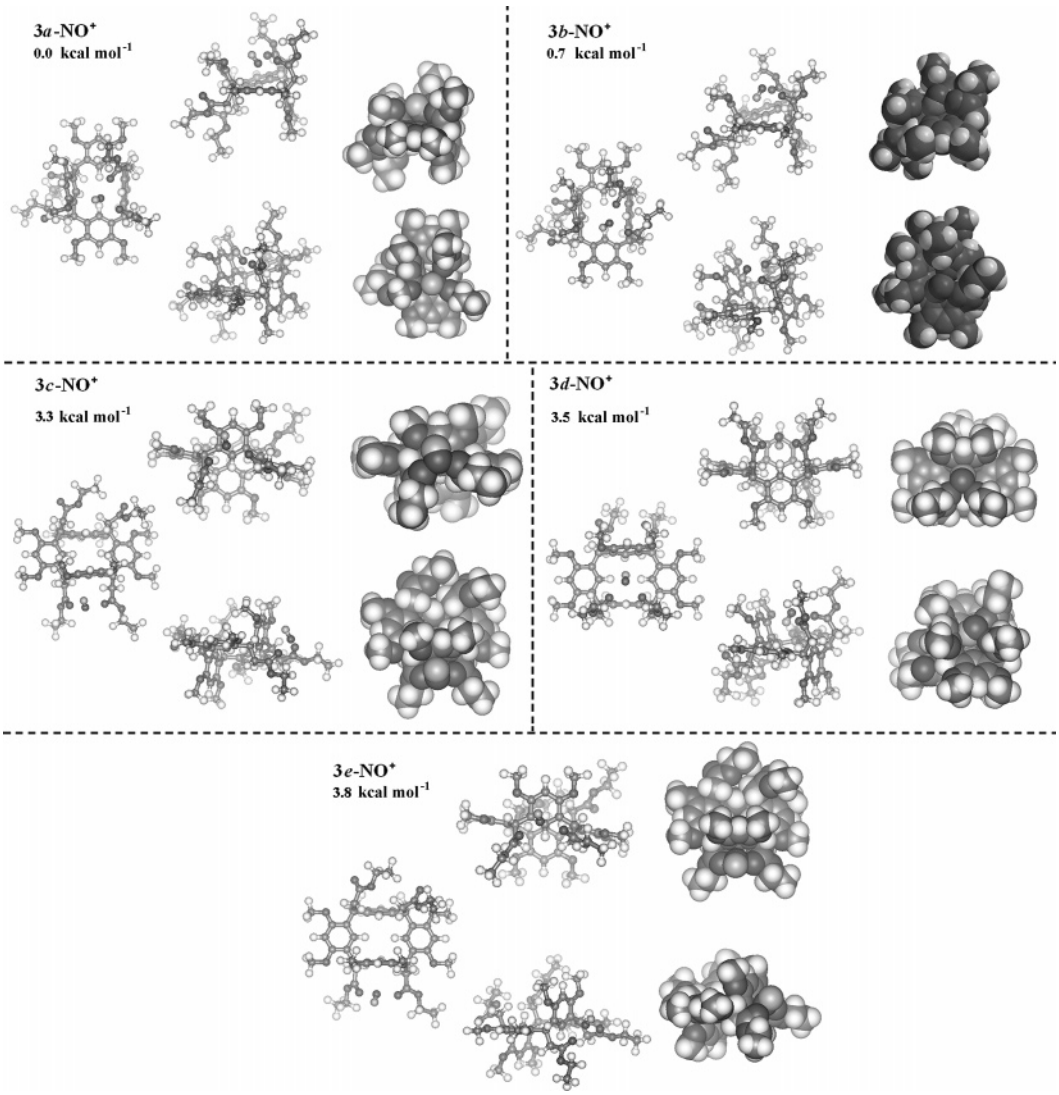

Figure 9. Ball-and-stick and CPK representations of the optimized geometries of **3**−NO^+ adducts obtained by semiempirical calculations. The energy values are relative to that of the most stable adduct **3*a***−NO^+.

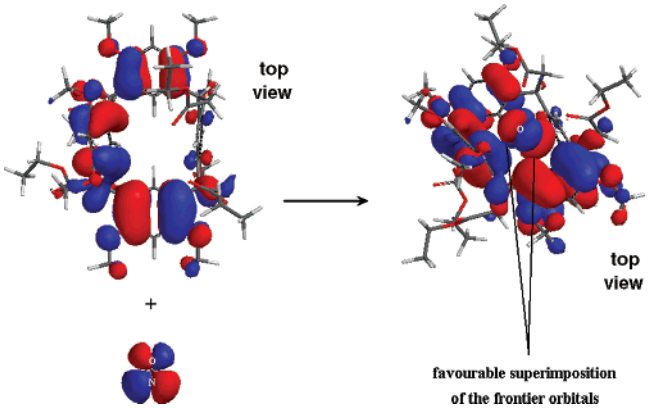

Figure 10. Pictures showing the favorable interactions between HOMO (host **3**) and LUMO (guest NO^+) orbitals in the **3*a***−NO^+ calculated adduct.

step, followed by a slower rearrangement toward more stable adducts. Although the formation kinetics appears less complicated for **3**−NO^+ than for **1**−NO^+, very similar rate constants were found (see Table 2) for the first (I for both the complexes) and the last step (III for **1**−NO^+ and II for **3**−NO^+), requiring for the establishment of the respective equilibria almost the same times, temperature, and concentrations of host and guest.

With regard to the ^{1}H NMR analysis of **3**−NO^+, the precipitation with hexanes gave, as did for **1**, a deeply colored, moisture-sensitive solid, enriched with the **3**−NO^+ complex. Indeed, in the ^{1}H NMR spectrum of the precipitate, the new signals, attributable to the complex, could be again easily distinguished (see Table 3). The distribution pattern of the signals for the aromatic protons remained the same as for the guest-free **3**, but those for H_i-25/27 and H_i-26/28 protons were shifted downfield (0.47 and 0.18 ppm, respectively), whereas those for H_e-11/23 and H_e-5/17 (at δ 6.39 and 6.46 ppm, respectively) were only slightly changed (to δ 6.41 and 6.42 ppm, respectively). Conversely, the two singlets at δ 3.88 and 3.65 ppm for the methoxyl groups in guest-free **3** were transformed into four singlets in the proton spectrum of **3**−NO^+. Moreover, the signals for the remaining aliphatic protons showed a 1:2:1 distribution (occasionally 3:1 for the methyl groups of the side-chains); for instance, the signal at δ 5.01 (dd, $J = 9$ and 6.5 Hz) of the bridge methine protons (2, 8, 14, 20) in resorcarene **3** was modified in the **3**−NO^+ complex into a set of signals at δ 5.47 (t, $J = 8$ Hz), δ 5.12 (t, $J = 8$ Hz), and δ

5.09 (m), the last with double intensity. These findings are in agreement with a C_S symmetry, which requires the presence of only one symmetry plain passing through two opposite methines bridge (e.g., C-2, C-14). The split of the chemical shifts for the side-chains protons is in accordance with the participation of the substituents to the entrapment of NO^+, but the signals distribution pattern can be explained by the presence of two different forms in a 1:1 equilibrium mixture: the up side-chains (on the same side of NO^+) would give one signal per form, whereas the quasi equivalent far down substituents would account for the signal with double intensity. The two forms are adequately represented by the calculated **3*a***−NO^+ and **3*b***−NO^+ geometries (Figure 9).

Because in NO^+-organic molecule interactions the formation of covalent products by oxidative dealkylations,[17] rearrangements involving the ester C=O fragments,[18] aromatic electrophilic NO^+ substitutions,[19] or oxidative aromatic nitrations[20] have been reported, the ^{1}H NMR spectra of the bleached solutions (upon addition of methanol or water) were examined and the parent resorc[4]arene (**1**−**3**) was recovered (92−95%) in each case.

Host−Guest Complexation with a 10-Fold Excess Guest to Host. The UV−vis spectra of three mixtures of resorc[4]arenes **1**−**3** with excess $NOBF_4$ were registered as a function of time (Figure 7S in Supporting Information). The large excess of NO^+ drastically reduced the absorptions in the LEB zone in all cases, as evidenced by the comparison with spectra of the same resorc[4]arenes at the same concentration, but with a host-to-guest excess. By the same way, a fast growth of the absorptions in the HEB zone was observed. These findings are in agreement with the results obtained by Kochi *et al.*[15] about the formation of complexes between aromatic compounds as donors and excess NO^+ as acceptor. Because the growth of the absorbance ratio between HEB and LEB bands by the increase of the guest concentration could be interpreted either as due to the formation of complexes with a guest/host ratio greater than 1:1 or to electrophilic aromatic substitutions, or both, an exhaustive discussion will be the subject of a separate paper.

Conclusions

The above results point out the great capability of resorc[4]arenes **1**−**3** in performing stable adducts with NO^+, independently on the host conformation, even though not-well-defined cavities among the aromatic rings are present, as in the case of **3**. Semiempirical calculations evidenced three optimized geometries of **1**−NO^+ complexes: two very stable and highly populated geometries (**1*a***−NO^+ and **1*b***−NO^+), featuring the guest inside the cavity, and a third less-stable geometry (**1*c***−NO^+), with the guest located outside, under the convex side of the resorcarene in the *lower rim* defined by the side-chain substituents. For host **2**, the **2*c***−NO^+ adduct with external NO^+ coordinated by the ester carbonyl groups was shown to be the most stable geometry, in agreement with the observed UV−vis spectral profile in the HEB zone. In the case of host **3**, three of the most stable geometries (**3*a***−NO^+, **3*b***−NO^+, and **3*d***−NO^+) placed NO^+ at the same time over the plain of the two horizontal aromatic rings and among one of the vertical aromatic rings and two ester carbonyl groups of the side-chains. The similarity kinetically observed in the NO^+-complexes typology between resorc[4]arenes **2** and **3** (same side-chains) rather than between **1** and **2** (same conformation) highlights the prominent role played by the nature of the substituents in the complexation. Halogen groups in the side-chains do not help (or help only partially, as in the case of the **1*c***−NO^+ adduct); conversely, the two ester carbonyl groups of adjacent side-chains are engaged to coordinate and capture the NO^+ cation. The resorcarene conformation is helpful, not as much as it resembles a cavity, but because it brings two methoxyl groups that may either promote the electron-donor capacity of the aromatic ring in charge-transfer interactions or drive the coordination of the NO^+ cation forward the host.

Experimental Section

General Remarks. ^{1}H NMR and ^{13}C NMR spectra were recorded at 298 K on a Bruker Ultra Shield 400 MHz spectrometer. UV−vis absorption spectra were recorded on a JASCO V-500 spectrometer. Parent resorc[4]arenes **1**−**3** used as hosts were prepared as previously described.[14a,14b] NO_2/N_2O_4 was generated from copper[7b] and concentrated HNO_3. ***Caution:*** *NO_2 has an irritating odor and is very toxic.* Semiempirical calculations were performed using Spartan 04 program with AM1 empirical system (see also Supporting Information). Potential surfaces were obtained through molecular modeling using Amber* Force Field. High-resolution mass spectra were obtained by FT-ICR-ESI on an APEX II spectrometer & Xmass software (Bruker Daltonics) − 4.7 T Magnet (Magnex).

General Procedure for the Preparation of Resorc[4]arene−Nitrosonium Complexes. Solutions of $NOBF_4$ (Aldrich) and resorc[4]arenes **1**−**3** were prepared in freshly distilled HPLC grade $CHCl_3$ (amylene stabilized 0.1%) under a nitrogen atmosphere, into an isolated glove box, at room temperature. Complexes **1**−NO^+, **2**−NO^+, and **3**−NO^+ were obtained upon mixing known amounts of both solutions (generally [host]/[NO^+] = 1:10 and [host]/[NO^+] = 10:1 ratios were reached). For the ^{1}H NMR analysis, the above solutions were prepared in $CDCl_3$ 99.9% (Aldrich). ^{1}H NMR signals were as given in Table 3.

FT-ICR-ESI-MS (pos.): **1**−NO^+, *m/z* found 1054.03501, $[C_{44}H_{52}Br_4NO_9]^+$ requires 1054.03701 (monoisotopic mass); **2**−NO^+, *m/z* found 974.41438, $[C_{52}H_{64}NO_{17}]^+$ requires 974.41688 (monoisotopic mass); **3**−NO^+, *m/z* found 974.41408, $[C_{52}H_{64}NO_{17}]^+$ requires 974.41688 (monoisotopic mass).

General Procedure for the UV−Vis Kinetic Studies. The experiments were divided into two sets, one with a [host]/[NO^+] = 10:1 ratio and the other with a [host]/[NO^+] = 1:10 ratio, to simplified the nonlinear curve fitting analysis for kinetic constants, simulating a pseudo-first-order trend, with the concentration of one of the two species kept constant during the time. Kinetic determinations are described in the Supporting Information.

For resorc[4]arene **1**, UV−vis spectra were acquired every 15 min for the first 4 h and then every 60 min for the following time. For the first kinetic phase, that occurred very quickly, data were recorded at just one wavelength (694 nm) every 30 s for the first hour. Concentrations in the following range were used: [**1**] = 3.50×10^{-2}−1.50×10^{-4} M; [NO^+] = 1.12×10^{-3}−1.30×10^{-2} M.

For resorc[4]arene **2**, UV−vis spectra were recorded at intervals of 3 min for the first 3 h, 50 min for the following 12 h, and 120 min for the remaining time. Concentrations in the following range were used: [**2**] = 1.32×10^{-2}−2.66×10^{-4} M; [NO^+] = 3.44×10^{-3}−1.30×10^{-3} M.

(17) Rathore, R.; Bosch, E.; Kochi, J. K. *Tetrahedron* **1994**, *50*, 6727−6758.
(18) (a) Kang, Y.; Zyryanov, G. V.; Rudkevich, D. M. *Chem.−Eur. J.* **2005**, *11*, 1924−1932 and references therein. (b) Pariiskii, G. B.; Gaponova, I. S.; Davydov, E. Ya. *Russ. Chem. Rev.* **2000**, *69*, 985−999. (c) Borodkin, G. I.; Shubin, V. G. *Russ. Chem. Rev.* **2001**, *70*, 211−230.
(19) Borodkin, G. I.; Elanov, I. R.; Andreev, R. V.; Shakirov, M. M.; Shubin, V. G. *Russ. J. Org. Chem.* **2006**, *42*, 406−411.
(20) Kim, E. K.; Kochi, J. K. *J. Org. Chem.* **1989**, *54*, 1692−1702.

For resorc[4]arene **3**, UV−vis spectra were recorded at intervals of 5 min for the first 4 h and 20 min for the following 20 h. Concentrations in the following range were used: [**3**] = 2.36×10^{-2}−0.74×10^{-3} M; [NO^+] = 1.22×10^{-3}−0.95×10^{-4} M.

CCDC-637642 contains the supplementary crystallographic data for this paper. These data can be obtained free of charge from The Cambridge Crystallographic Data Centre via www.ccdc.cam.ac.uk/datarequest/cif.

Acknowledgment. Financial supports by Università "La Sapienza", Roma, Italy (funds for selected research topics 2003−2005) and FIRB 2003 are acknowledged. This work was partially supported by the "Istituto Pasteur−Fondazione Cenci Bolognetti", Università "La Sapienza", Roma, Italy.

Supporting Information Available: Computational methods and kinetic determinations. Figures 1S−8S. Re-assignment of the conformation of compound **3** by X-ray analysis. This material is available free of charge via the Internet at http://pubs.acs.org.

JA072855I